Article

Hydrogenation of Anthracene in Supercritical Carbon Dioxide Solvent Using Ni Supported on Hβ-Zeolite Catalyst

Endalkachew Sahle-Demessie *, Venu Gopal Devulapelli and Ashraf Aly Hassan

U.S. Environmental Protection Agency, Office of Research & Development, National Risk Management Research Laboratory, 26 West, Martin Luther King Dr., Cincinnati, OH 45268, USA; E-Mails: venudevula@yahoo.com (V.G.D.); hassan.ashraf@epa.gov (A.A.H.)

* Author to whom correspondence should be addressed; E-Mail: sahle-demessie.endalkachew@epa.gov; Tel.: +1-513-569-7739; Fax: +1-513-569-7677.

Abstract: Catalytic hydrogenation of anthracene was studied over Ni supported on Hβ-zeolite catalyst under supercritical carbon dioxide (sc-CO_2) solvent. Hydrogenation of anthracene in sc-CO_2 yielded 100% conversion at 100 °C, which is attributed to the reduced mass transfer limitations, and increased solubility of H_2 and substrate in the reaction medium. The total pressure of 7 MPa was found to be optimum for high selectivity of octahydroanthracene (OHA). The conversion and selectivity for OHA increased with an increase in H_2 partial pressure, which is attributed to higher concentration of hydrogen atoms at higher H_2 pressures. The selectivity reduced the pressure below 7 MPa because of enhanced desorption of the tetrahydro-molecules and intermediates from Ni active sites, due to higher solubility of the surface species in sc-CO_2. The selectivity of OHA increased with the increase in catalyst weight and reaction time. The rate of hydrogenation of anthracene was compared with that found for napthalene and phenanthrene. The use of acetonitrile as co-solvent or expanded liquid with CO_2 decreased the catalytic activity.

Keywords: supercritical carbon dioxide; nickel/zeolite catalyst; anthracene; hydrogenation

1. Introduction

Cyclic saturated hydrocarbons are proposed as a new mobile hydrogen storage media for proton exchange membrane fuel cells [1–4]. A hydrogen storage system with cyclic saturated hydrocarbons is

more stable and inexpensive than systems with inorganic hydrogen-adsorbing alloys. Hydrogenation of aromatic compounds is important for the production of high performance diesel fuel (low aromatic diesel fuels) [5–8]. Polycyclic aromatic compounds (PAHs) are components of coal tar, creosote and crude oil, and are formed by incomplete combustion of organic materials. Because of their carcinogenic and mutagenic properties, PAHs are regarded as environmental priority pollutants [9,10].

In the past two decades, supercritical carbon dioxide (sc-CO_2) has emerged as an environmentally benign green solvent for performing hydrogenation of organic compounds, due to its low toxicity and cost resulting in little environmental burden compared to more expensive volatile organic solvents. The ability of the sc-CO_2 to dissolve many of reactive gases like H_2, O_2 and also a variety of organic compounds facilitates oxidation and hydrogenation reactions in this medium, thereby eliminating inter-phase mass transfer limitations and enhancing the reaction rate. The primary rationale for use of a sc-CO_2 as a solvent in hydrogenation reactions is the elimination of transport limitations, by improving the solubility of hydrogen in the reaction mixture.

sc-CO_2 medium has shown to be more favorable for hydrogenation, oxidation, alkylation and hydroformylation compared to the reactions in organic solvents [11,12]. Moreover, eliminating the use of organic solvent is highly desirable for environmentally benign processing. Near the critical point of the solvent, slight changes in temperature and pressure can change the activity and selectivity of the reaction significantly, which can provide a remarkable potential for its use. Phase control in sc-CO_2 is also used to separate the reaction products by means of pressure release. Several researchers have demonstrated the potential of sc-CO_2 as an alternative reaction medium for a variety of synthetic transformations including production of fine chemicals and pharmaceuticals [13–15]. Poliakoff *et al.* have reported hydrogenations of a variety of liquid compounds in sc-CO_2 medium over Deloxan aminopolysiloxane supported noble metal (Pd, Ru, Pt) catalysts [16] and Subramaniam *et al.* have reported fixed-bed hydrogenation of cyclohexene to cyclohexane in sc-CO_2 over Pd/C catalyst [17].

Shirai *et al.* [18], studied the hydrogenation of naphthalene and 1-naphthol over supported metal catalysts in sc-CO_2 solvent. Hiyoshi *et al.* [19], studied the tuning of cis-decalin selectivity in naphthalene hydrogenation over carbon-supported rhodium catalyst in sc-CO_2. Yuan *et al.* [20], reported the catalytic hydrogenation of poly cyclic aromatic hydrocarbons over palladium supported on γ-Alumina catalyst under mild conditions. Hydrogenation of polycyclic hydrocarbons such as naphthalene, anthracene and phenanthrene was carried out over metalloporphyrins by Nelkenbaum *et al.* [21]. Hydrogenation activity increased in the order of naphthalene < phenanthrene < anthracene. Di-, tetra-, octahydrogenation products were obtained for anthracene hydrogenation.

The present study aims at fine tuning reaction conditions for the catalytic hydrogenation of anthracene over nickel supported on Hβ-zeolite catalyst using supercritical carbon dioxide as solvent. Reaction conditions studied need to be optimized with respect to pressure, hydrogen concentration, catalyst weight and reaction time. The use of sc-CO_2 is limited by inadequate reaction solubilities, and the need for high pressure to obtain sufficient reaction rates, may cause high capital and operating costs. The application of CO_2 expanded acetonitrile mixed binary solvent composed of CO_2 condensed into an organic solvent, would have the benefits of high solubility of the organic liquid and improved transport properties of the sc-CO_2 [22]. In this study we also looked at the use CO_2 expanded acetonitrile for the hydrogenation of anthracene.

2. Results and Discussion

2.1. Catalyst Characterization

The X-ray diffraction patterns of Ni supported on H-β zeolite are shown in Figure 1. The peaks located in the region of 5° < 2θ < 35° are representative peaks of a typical H-β zeolite. The peaks at 2θ = 43.26°, 62.73°, 75.38° and 79.9° are representative peaks of a nickel oxide. As can be seen in Figure 1, the intensity of peaks corresponding to H-β zeolite decreased, whereas, the intensity of peaks corresponding to nickel oxide increased on increasing the nickel loading on H-β zeolite.

Figure 1. X-ray diffraction patterns of Ni/Hβ-zeolite catalysts with increasing nickel loading.
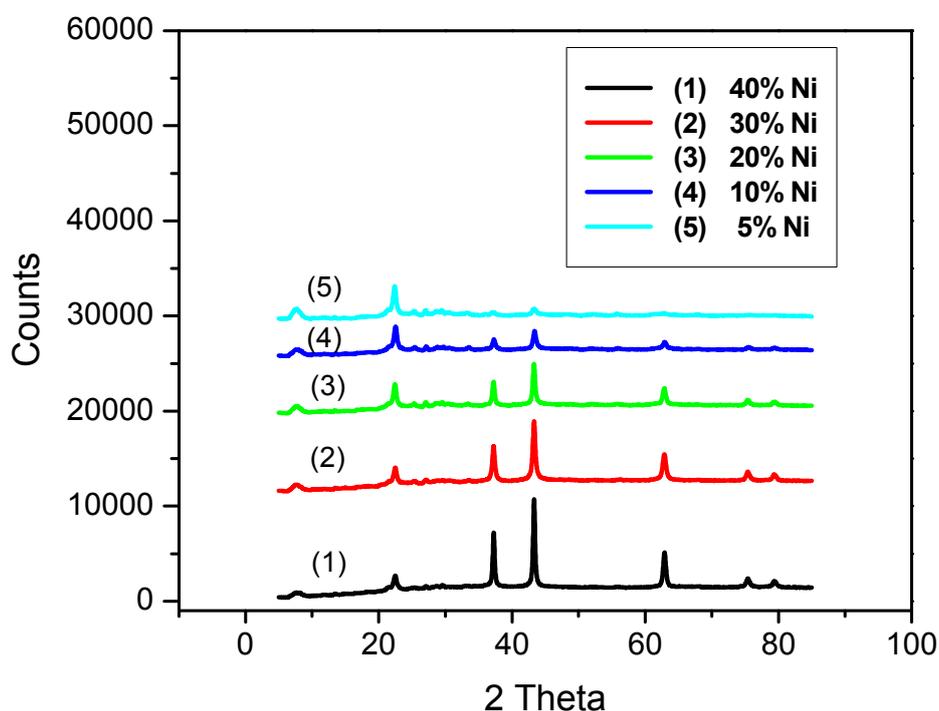
The BET surface areas of nickel supported Hβ-zeolite catalysts are given in Table 1. The surface areas of the Ni/Hβ-zeolite catalyst decreased with increased nickel loading. This decrease is expected since the impregnation of low surface area materials onto a high surface area porous H-β zeolite decreases the surface area of the latter.

Table 1. Physicochemical property of Ni/Hβ-zeolite catalysts.

Sample Number	Catalyst	BET-SA ($m^2 \cdot g^{-1}$)	T_{max} °C	H_2 uptake mMol	T_{max} °C	H_2 uptake mMol	Total H_2 uptake mMol
1	5% Ni-Hβ	258	354	118	478	95	214
2	10% Ni-Hβ	163.65	217	41	525	102	321
			372	178			
3	20% Ni-Hβ	141.6	376	416	498	86	502
4	30% Ni-Hβ	95.6	389	716	577	33	749
5	40% Ni-Hβ	50.6	382	801	530	36	838

Figure 2. Temperature programmed reduction (TPR) patterns of Ni/Hβ-zeolite catalysts.
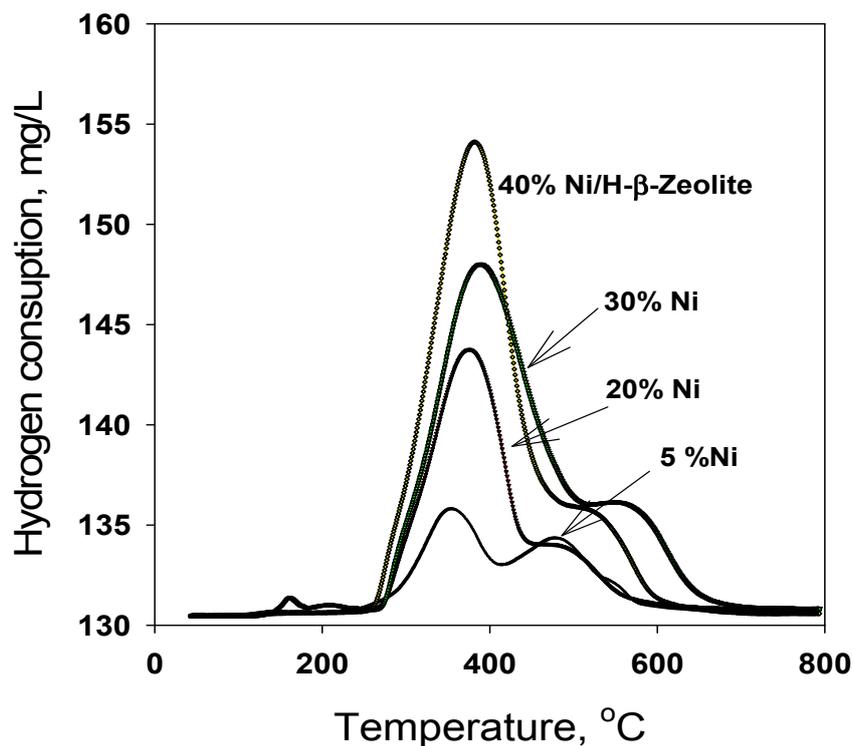
The reducibilities of the nickel phases over the catalysts were investigated by TPR technique. The TPR profiles of the Ni/H-β-Zeolite catalysts are shown in Figure 2. As can be observed, the four peaks overlapped and these peaks shift to higher temperatures as the nickel loading increases. The first peak at temperature less than 420 °C, corresponds to a typical reduction of the supported nickel oxide, *i.e.*, supported nickel oxide present on the outer surface of the zeolite. The second peak accounts for nickel in Ni-zeolite that is reducible above 500 °C [23,24]. Others have also observed that the reduction of NiO bulk occurs at 220 to 420 °C [25,26]. Pedrosa *et al.* [27] studying TPR of nickel on H Y zeolite, suggested that the different reduction temperatures for Ni^{2+} corresponded to the location of cations in the zeolite. The first and second peaks of nickel reduction, at 238 and 507 °C, are attributed to the reduction of Ni^{2+} species located in the sodalite and hexagonal cavities, respectively. The ratios of the areas for the peaks with a maximum near 400 °C with that around 520 °C, is 1.6. Thus the TPR data suggests that more than 60% of the nickel oxide is located on the external surface of the support. The TPR peaks at temperatures above 500 °C may correspond to the reduction of nickel particles located inside the cavities of the zeolite, including the channels and cages of the structure. The differences in TPR profiles may be due to nickel species being present in the cavities and/or on the surface of the zeolite catalyst supported.

It could also be observed that the number of diffraction peaks did not change with respect to H-β-Zeolite, indicating that no crystalline transformation occurred during metal impregnation. The XRD pattern of 5% nickel loading on H-β-Zeolite shows the peak intensity was strong at $2\theta = 22$ and weak at $2\theta = 38$, 43, and 62 (Figure 1). Most of the expected peaks could not be observed because of their low concentration or amorphous nature. Hydrogen consumption during TPR, in temperatures below 400 °C, showed strong interaction between NiO particles and H-β-Zeolite. Thus, these peaks can be associated with the reduction of nickel that interacts with zeolite in different intensities. The

reduction at profile of lower concentration nickel is in accordance with Rynkawski *et al.* [28], who observed a bimodal nature of nickel oxide species, which includes an amorphous over layer on nickel oxide that interacts but is not chemically bound with the support and reduced at lower temperatures and spinels of Ni-H-β-Zeolite oxides at higher temperatures.

2.2. Catalytic Activity

2.2.1. Effect of Reaction Temperature on Hydrogenation of Anthracene

Effect of temperature on hydrogenation of anthracene was studied in the range of 80–130 °C over 10 wt.% Ni/Hβ-zeolite. The results are shown in Figure 3. The conversion of anthracene increased from 32.4 to 59.8% with increased temperature from 80 °C to 130 °C.

Figure 3. Effect of temperature on hydrogenation of anthracene over 10 wt.% Ni/Hβ-zeolite catalyst. Catalyst weight: 0.5 g; Reaction pressure: 6.9 MPa; H_2 partial pressure: 2.76 MPa; volume of the reactor: 50 mL; reaction time: 6 h.
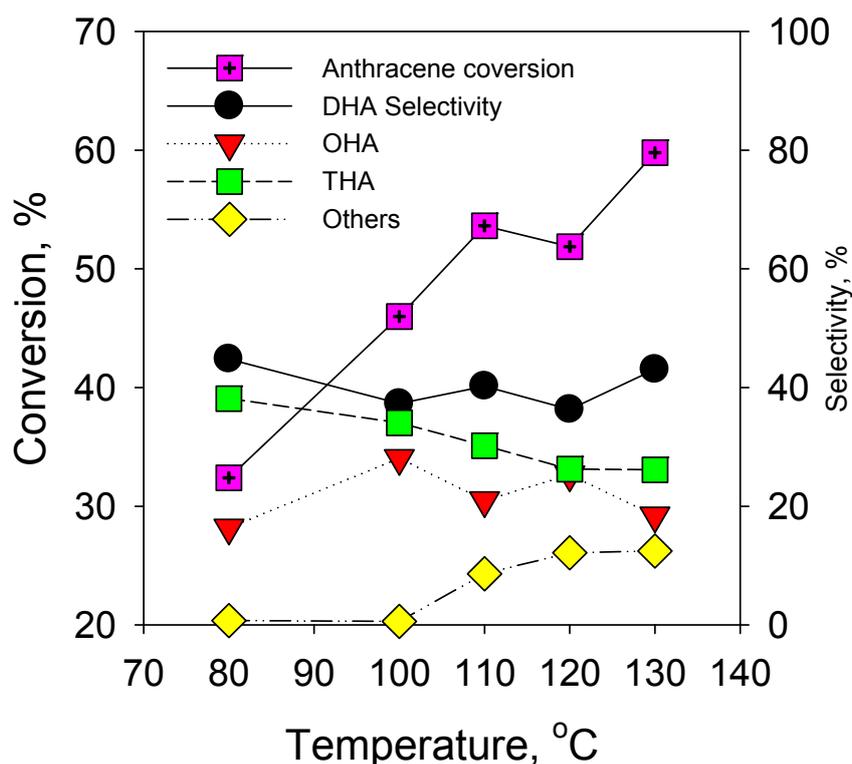

2.2.2. Effect of Nickel Loading on Hydrogenation of Anthracene

Although, the reaction medium is a mixture of CO_2 and H_2 the literature data indicates that the substrates have solubility around $(0.1–2) \times 10^{-4}$ mole fraction at reaction conditions [29,30]. The conversion of anthracene increased as the weight fraction of Ni on Hβ-zeolite support increased from 5 wt.% to 40 wt.% (Figure 4). This indicates the conversion of anthracene improves with the increase in the number of active sites on the catalyst. The TPR studies of the catalyst indicated the hydrogen uptake by the catalyst, in turn, the number of active sites, increased on increasing the wt.% of nickel on the support. The catalytic activity results are in correlation with hydrogen uptake of the catalyst.

Meanwhile, the selectivity of the products did not change significantly with increasing the nickel loading on Hβ-zeolite support. The results indicate that using sc-CO_2 as a solvent 100% hydrogenation of anthracene was achieved at 100 °C over 40 wt./% Ni/Hβ-zeolite, which is attributed to the reduced mass transfer limitations, and increased solubility of H_2 and substrate in the dense CO_2 medium.

Figure 4. Effect of metal loading on hydrogenation of anthracene. Catalyst weight: 0.5 g; Reaction temperature: 100 °C; Reaction pressure: 6.9 MPa; H_2 partial pressure: 2.76 MPa; volume of the reactor: 50 mL; reaction time: 6 h.
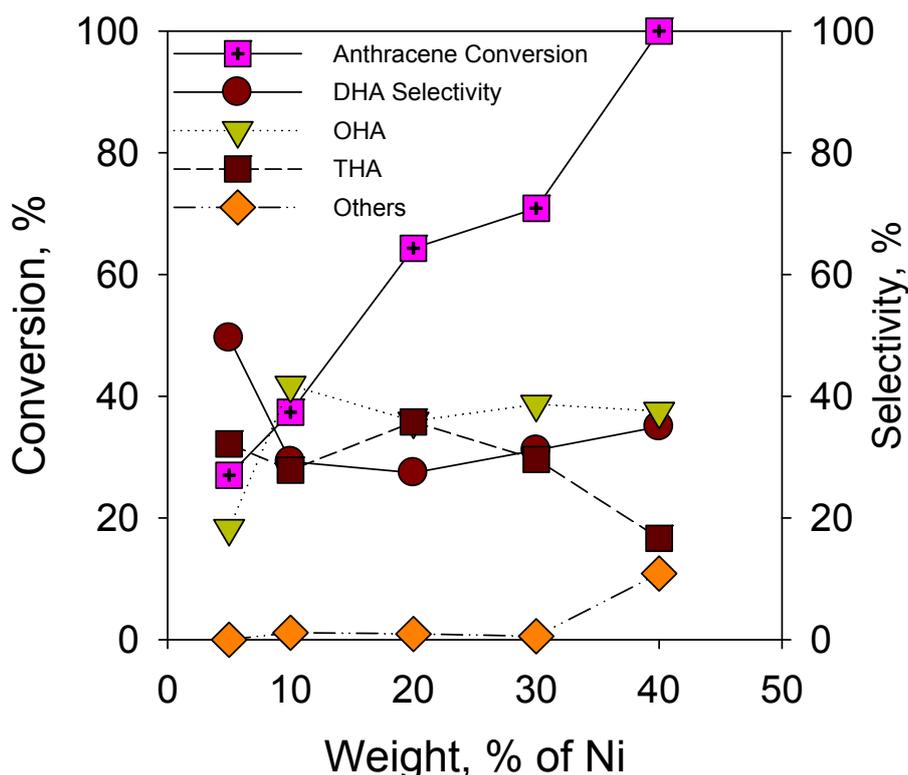
2.2.3. Effect of Reaction Pressure on Hydrogenation of Anthracene

The effect of reaction pressure on hydrogenation of anthracene was studied from 2.8–16.6 MPa and the results are shown in Figure 5. The conversion anthracene is almost 100% in all cases, except at 2.76 MPa reaction pressure where the conversion was 94%. It is interesting to see in the figure that the selectivity of octahydroanthracene increased with increasing reaction pressure in the range of 2.8–6.9 MPa and decreased beyond 6.9 MPa. The results indicate that tetrahydroanthracene is the predominant product at low reaction pressure and is further hydrogenated to octahydroanthracene with increasing reaction pressure up to 6.9 MPa. Higher pressures above 6.9 MPa showed no significant effect on the reaction. The total pressure of 6.9 MPa was found to be optimum for the high selectivity of octahydroanthracene. The drop in selectivity beyond 6.9 MPa could be explained by the enhanced desorption tetrahydro-molecules and intermediates from Ni active sites due to higher solubility of surface species in sc-CO_2. Hiyoshi *et al.* [31], observed the same effect while studying hydrogenation of biphenyl over supported transition metal catalyst under sc-CO_2 solvent.

Figure 5. Effect of reaction pressure on hydrogenation of anthracene over 40% Ni/Hβ-zeolite catalyst. Catalyst weight: 0.5 g; Reaction temperature: 100 °C; H$_2$ partial pressure: 2.76 MPa; volume of the reactor: 50 mL; reaction time: 6 h.
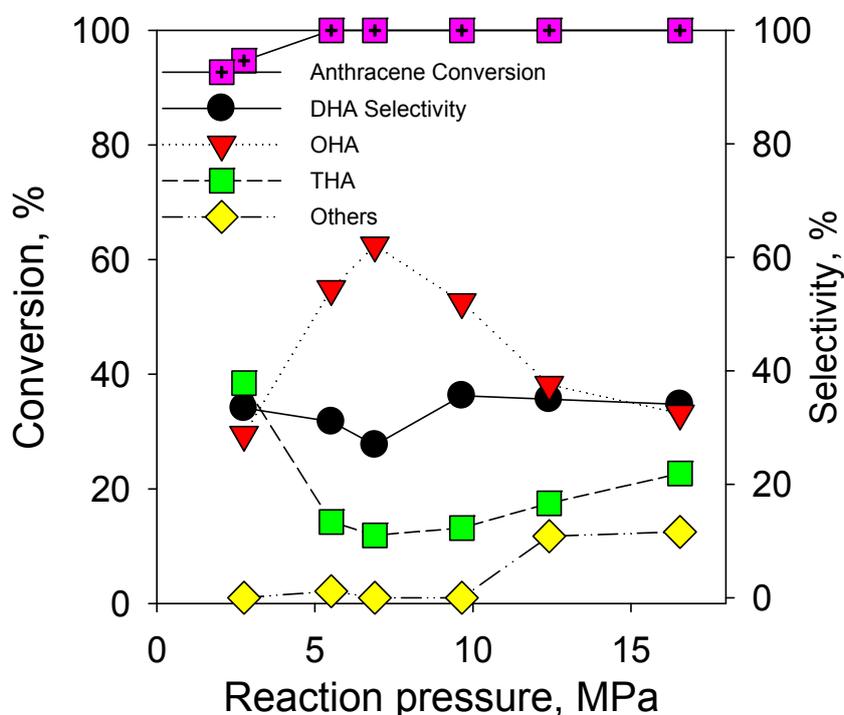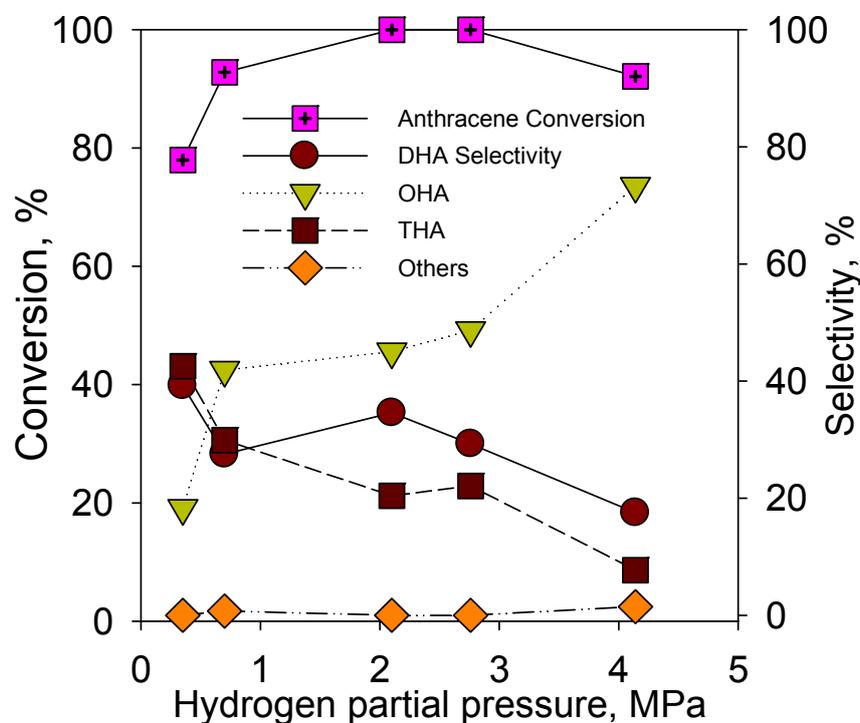

2.2.4. Effect of Hydrogen Partial Pressure on Hydrogenation of Anthracene

The effect of hydrogen partial pressure on hydrogenation of anthracene was studied from 0.35–4.1 MPa hydrogen partial pressure and the results are presented in Figure 6. The results shown in Figure 6 indicate that the conversion of anthracene increased on increasing hydrogen partial pressure. The selectivity for dihydroanthracene and tetrahydroanthracene decreased, whereas the selectivity for octahydroanthracene increased on increasing the hydrogen partial pressure. This implies the degree of hydrogenation improves with increasing the hydrogen partial pressure. The increase in the concentration of hydrogen around the active sites is responsible for the increase in the degree of hydrogenation and these results are in agreement with results reported in the literature [18,19,30]. At the hydrogen partial pressure of 4 MPa there was a moderate decrease in the conversion of the total hydrogenation of anthracene, although the patterns in selectivities did not change. This might be caused by the changes in the phase behavior of hydrogen-CO$_2$-anthracene mixture, however further investigation is needed.
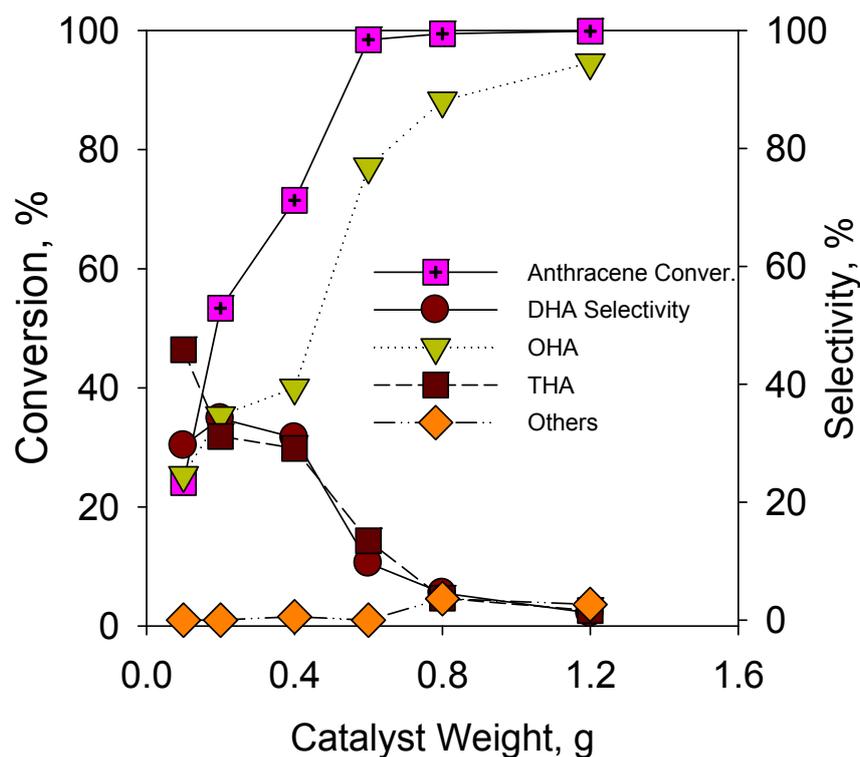
2.2.5. Effect of Catalyst Weight on Hydrogenation of Anthracene

Figure 7 presents the effect of catalyst weight on hydrogenation of anthracene. The conversion of anthracene and the selectivity for octahydroanthracene increased with increasing amount of catalyst. The increase for active sites as a result of increased catalyst concentration is responsible for the increased activity and selectivity. It could be understood from the results presented that the reaction is not mass transfer controlled at reaction conditions studied.

Figure 6. Effect of hydrogen partial pressure on hydrogenation of anthracene over 40% Ni/Hβ-zeolite catalyst. Catalyst weight: 0.5 g; Reaction temperature: 100 °C; Reaction pressure: 6.9 MPa; volume of the reactor: 50 mL; reaction time: 6 h.


Figure 7. Effect of catalyst weight on hydrogenation of anthracene over 40% Ni/Hβ-zeolite catalyst. Reaction temperature: 100 °C; Reaction pressure: 6.9 MPa; H_2 partial pressure: 2.76 MPa; volume of the reactor: 50 mL; reaction time: 6 h.

2.2.6. Effect of Reaction Time on Hydrogenation of Anthracene

The effect of reaction time on the hydrogenation of anthracene was studied over 40 wt.% Ni/H-β zeolite and the results are shown in Figure 8. Longer reaction times improved the conversion of anthracene. It is interesting to see that the selectivity of octahydroanthracene increased and the selecetivities of di-, and tetrahydroanthracene decreased with increased reaction time. This indicates the di-, and tetrahydroanthracene formed were converted to octahydroanthracene on increasing the reaction time.

Figure 8. Effect of reaction time on hydrogenation of anthracene over 40% Ni/Hβ-zeolite catalyst. Catalyst weight: 0.5 g; Reaction temperature: 100 °C; Reaction pressure: 6.9 MPa; H_2 partial pressure: 2.76 MPa; volume of the reactor: 50 mL; reaction time: 6 h.
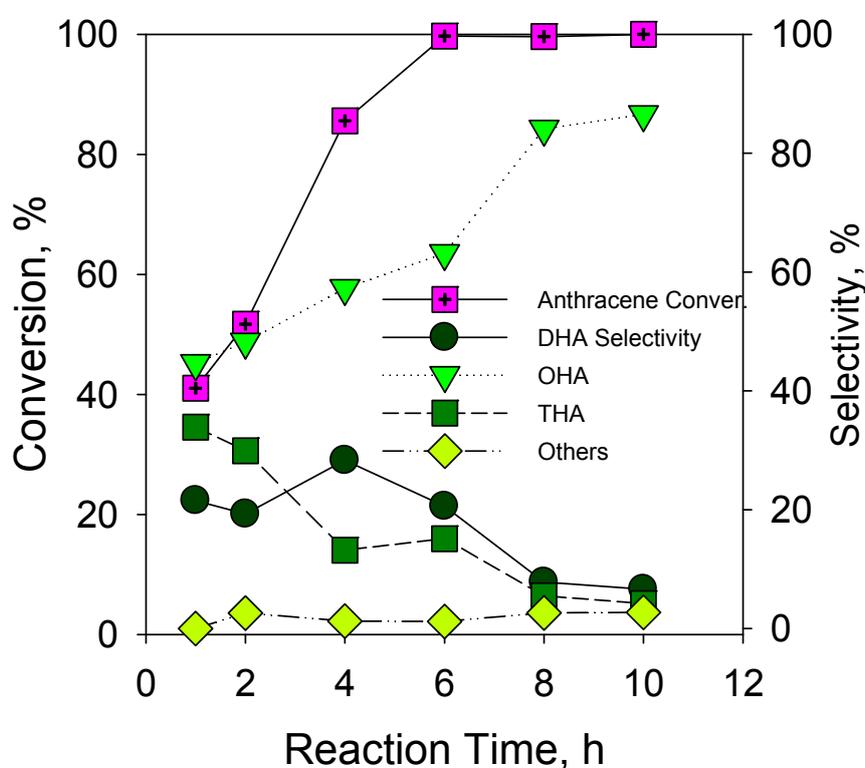

2.2.7. Effect of Solvent on Hydrogenation of Anthracene

The effect of solvent on hydrogenation of anthracene was carried out at 100 °C over 10 wt.% Ni/Hβ-zeolite and the results are shown in Figure 9. The reaction carried out under nitrogen pressure showed less conversion of anthracene compared to the reaction carried at the same amount of carbon dioxide pressure. This indicates that the sc-CO_2 eliminates the transport limitations, by improving the solubility of hydrogen at the reaction mixture. Whereas, the reactions carried under acetonitrile and sc-CO_2 expanded acetonitrile showed almost negligible conversions of anthracene. The low catalytic activity in sc-CO_2 expanded acetonitrile might be due to the fact the specific solvation of carbon dioxide molecule for anthracene suppressed by co-solvent. Aizawa *et al.* [32], reported the co-solvent shields specific interaction between solute and the CO_2 solvent. Moreover, we observed the

hydrogenated products of acetonitrile such as ethylamine, diethylamine and triethylamine, which may have a poisoning effect on the catalyst.

Figure 9. Effect of solvent on hydrogenation of anthracene over 10 wt.% Ni/Hβ-zeolite catalyst. Catalyst weight: 0.5 g; Reaction temperature: 100 °C; Reaction pressure: 6.9 MPa; H_2 partial pressure: 2.76 MPa; volume of the reactor: 50 mL; reaction time: 6 h.
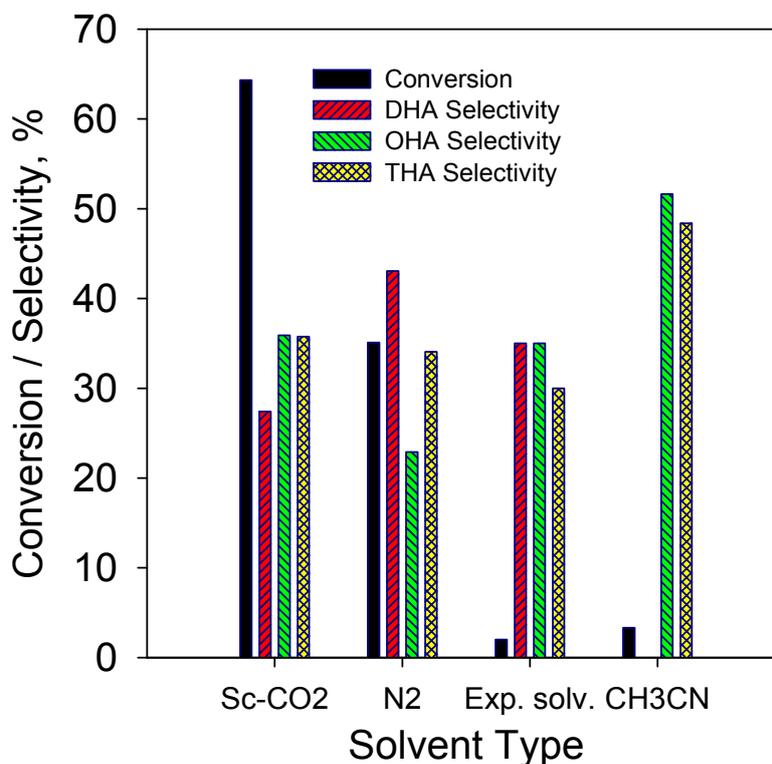
2.2.8. Reaction Mechanism of Anthracene Hydrogenation

A scheme of reaction mechanism of hydrogenation of anthracene based on the product distribution is shown in Scheme 1. Although more than twelve products were detected including 1,2,3,4-tetrahydroanthracene that are present in trace quantity at lower reaction temperatures, four isomers of octahydroanthracene, and six isomers pf tetradecahydroanthracene, we only report the major products. Hydrogenation of anthracene results mainly in the formation of di- and tetrahydroanthracene which were further hydrogenated to octa-hydroanthracene as a major product. In order to understand the reaction pathway, the hydrogenation of di-, tetra- and octahydroanthracene were carried out. The hydrogenation of di- and tetrahydro anthracene completely converted to octahydroanthracene whereas, no conversion was obtained from octahydroanthracene. The results indicate that dihydroanthracene can be either directly converted and/or via tetrahydroanthracene to octahydroanthracene.

**Scheme 1.** Reaction pathway for hydrogenation of anthracene.
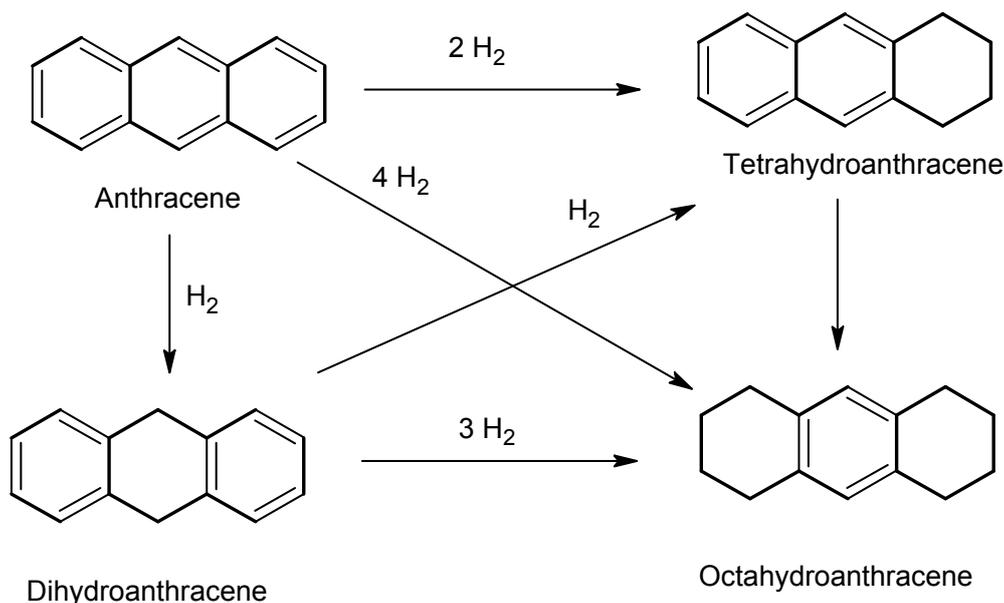
2.2.9. Comparison of Reaction Kinetics of Hydrogenation Anthracene with Phenanthrene and Naphthalene

A plot of $-\ln(1 - X)$ *versus* reaction time, where X is fractional conversion of anthracene, for anthracene hydrogenation reactions carried out at 90°, 100° and 110 °C showed a near linear character. This suggests a first-order dependence of the rate of the reaction on anthracene concentration. Hence, the rate expression for anthracene (M) can be written as:

$$-r_M = k\,C_M \tag{1}$$

The reaction rate constants calculated from the slopes of plots in Figure 10 are 2.7×10^{-3} min^{-1}, 11.9×10^{-3} min^{-1} and 12.8×10^{-3} for anthracene hydrogenation at 90°, 100° and 110 °C, respectively. A plot of $-\ln(1 - X)$ *versus* reaction time, where X is fractional conversion of phenanthrene, for phenanthrene hydrogenation reactions carried out at 90°, 100° and 110 °C showed a near linear character with the R-square values of 0.85, 0.93, and 0.95, respectively (Figure 11). The reaction rate constants calculated from the slopes of plots in Figure 11 are 0.3×10^{-3}, 0.3×10^{-3} and 0.5×10^{-3} min^{-1} for phenanthrene hydrogenation at 100°, 120° and 130 °C, respectively. The goodness of fit for the first-order model for three isothermal reactions is given by R-square values of 0.85, 0.93, and 0.95, respectively. Moreover, negligible conversions were obtained during the hydrogenation of naphthalene. The hydrogenation activity of polycyclic aromatic compounds followed the order naphthalene < phenanthrene < anthracene. The same trend was observed by Nelkenbaum *et al.* [21].

Figure 10. First-order dependence plot for hydrogenation of anthracene at 90 °C, 100 °C and 110 °C over 40 wt.% Ni/Hβ zeolite catalyst. Catalyst weight: 0.5 g; Reaction pressure: 6.9 MPa; H_2 partial pressure: 2.76 MPa; volume of the reactor: 50 mL.
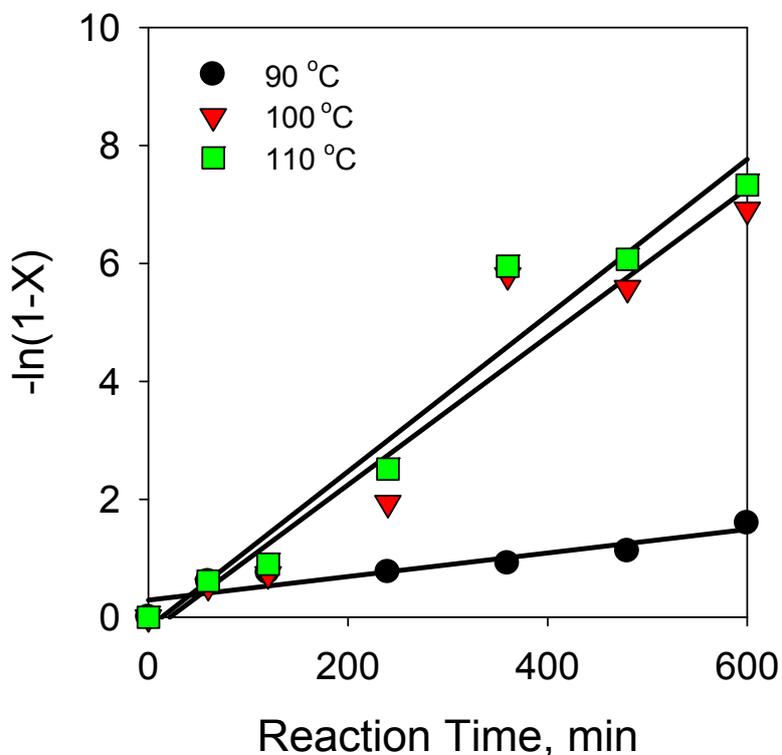
Figure 11. First-order dependence plot for hydrogenation of phenanthrene at 100 °C, 120 °C and 130 °C over 40 wt.% Ni/Hβ zeolite catalyst. Catalyst weight: 0.5 g; Reaction pressure: 6.9 MPa; H_2 partial pressure: 2.76 MPa; volume of the reactor: 50 mL.
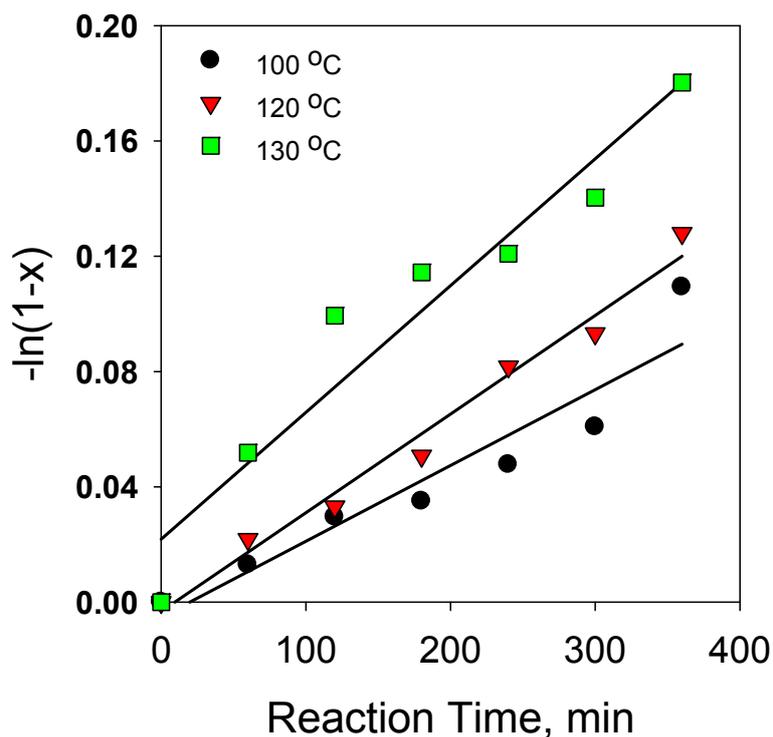
3. Experimental Section

3.1. Catalyst Preparation

Ni supported on Hβ-zeolite catalysts was prepared by impregnation method. A typical procedure for the impregnation involves the soaking of Hβ-zeolite powder in aqueous solutions of nickel nitrate in appropriate mole ratios for 2 h followed by evaporating the water on a hot plate under constant stirring. The metal oxide impregnated catalyst was obtained by drying this material in vacuum oven at 110 °C for 6 h followed by calcination in air at 450 °C for 4 h at a temperature ramp of 10 °C/min. Prior to hydrogenation, the calcined catalyst was reduced under hydrogen flow of 30 mL/min at 450 °C for 4 h at a temperature ramp of 10 °C/min.

3.2. Catalyst Characterization

The calcined catalysts were characterized using powder X-ray diffraction (XRD), BET surface area, and TPR techniques. Powder diffraction patterns were recorded on a GBC Minimaterial analyzer (Australia) using Cu K_α radiation source. Scans were performed over the 2θ range from 5° to 90° at 0.02 stepsize and 1 degree/min scan speed and 1 kW power.

The BET surface areas of the catalysts were measured using nitrogen adsorption at 77 K on a Micromeretics (AutoChem 2920, Norcross, GA, USA) surface area analyzer. Prior to analyses, 0.35 g of sample catalysts were loaded into a quartz reactor and degassed at 120 °C with a helium purge for 60 min. A single-point nitrogen adsorption isotherm was used to determine the BET surface area of the sample. Temperature programmed reduction (TPR) analyses of the catalysts were performed on a Micrometric Autochem 2920 instrument using hydrogen as a reducing gas. The catalyst (0.35 g) was charged into a U-tube reactor and pretreated in oxygen at 450 °C for 2 h. TPR was performed at heating rates of 10 °C/min up to 800 °C under a flow of 11.2% H_2/Ar (50 cm^3/min). The temperature was decreased to ambient and then the temperature was increased at temperature ramp of 10 °C to 600 °C under hydrogen flow. The consumption of hydrogen was monitored by a thermal conductivity detector (TCD) and recorded at a signal rate of 5 points/min. The hydrogen consumption was quantified by a pulse calibration. The temperature was measured adjacent to the catalyst bed and followed a strictly linear trend.

3.3. Catalytic Reactions

The catalytic hydrogenation of anthracene over Ni/Hβ-zeolite catalysts was carried out in a 50 mL stainless steel reactor equipped with temperature controller, pressure sensor and a furnace. Before the reaction, the catalyst was reduced at 450 °C for 4 h. 0.5 g of the pre-reduced catalyst and 0.01 mol (1.78 g) of anthracene were quickly added to the reactor. The reactor was flushed three times with hydrogen to remove air from the reactor and the reaction temperature was raised to 100 °C. Then the reactor was filled with 2.76 MPa of hydrogen and 6.9 MPa of carbon dioxide pressure. After the reaction, the reactor was cooled to room temperature and vented slowly. View cell was used to verify that the density of the sc-CO_2 was sufficient to ensure that the reactants are substantially in a single phase. The products were collected and analyzed by a Hewlett-Packard 6890 Gas Chromatograph

using a HP-5 Capillary Column. (30 m × 320 m × 0.25 m) and a quadruple mass filter equipped HP 5973 mass selective detector under a temperature programmed heating from 40 to 200 °C at 10 °C/min. Quantification of each product was obtained using a multi-point calibration curve for each product.

4. Conclusions

XRD analyses showed the main peaks and bands characteristic of the structure in all samples. TPR profiles showed two peaks for nickel reduction in Ni*/H-β-zeolite. Higher density of acid sites was obtained on Ni*/H-β-zeolite.

Hydrogenation of anthracene in sc-CO_2 as solvent gave 100% conversion at 100 °C which is attributed to the reduced mass transfer limitations, and increased solubility of H_2 and substrate in dense CO_2 medium. The total pressure of 6.9 MPa was found to be optimum for the high selectivity of octahydroanthracene. The conversion and selectivity of octahydroanthracene increased with the increase in H_2 partial pressure, which is attributed to the higher concentration of hydrogen atoms at higher H_2 pressures. The selectivity of octahydroanthracene increased with the increase in catalyst weight and reaction time. The use of acetonitrile as co-solvent decreased the catalytic activity.

References

1. Alhumaidan, F.; Cresswell, D.; Garforth, A. Hydrogen storage in liquid organic hydride: Producing hydrogen catalytically from methylcyclohexane. *Energy Fuels* **2011**, *25*, 4217–4234.
2. Hodoshima, S.; Arai, H.; Takaiwa, S.; Saito, Y. Catalytic decalin dehydrogenation/naphthalene hydrogenation pair as a hydrogen source for fuel-cell vehicle. *Int. J. Hydrog. Energy* **2003**, *28*, 1255–1262.
3. Kariya, N.; Fukuoka, A.; Ichikawa, M. Efficient evolution of hydrogen from liquid cycloalkanes over pt-containing catalysts supported on active carbons under "wet-dry multiphase conditions". *Appl. Catal. A* **2002**, *233*, 91–102.
4. Wang, Y.; Shah, N.; Huffman, G.P. Pure hydrogen production by partial dehydrogenation of cyclohexane and methylcyclohexane over nanotube-supported pt and pd catalysts. *Energy Fuels* **2004**, *18*, 1429–1433.
5. Zieliński, M.; Pietrowski, M.; Wojciechowska, M. New promising iridium catalyst for toluene hydrogenation. *ChemCatChem* **2011**, *3*, 1653–1658.
6. Cooper, B.H.; Donnis, B.B.L. Aromatic saturation of distillates: An overview. *Appl. Catal. A* **1996**, *137*, 203–223.
7. Huang, T.-C.; Kang, B.-C. Naphthalene hydrogenation over pt/al2o3 catalyst in a trickle bed reactor. *Ind. Eng. Chem. Res.* **1995**, *34*, 2349–2357.
8. Qian, W.; Shirai, H.; Ifuku, M.; Ishihara, A.; Kabe, T. Reactions of tetralin with tritiated molecular hydrogen on pt/al2o3, pd/al2o3, and pt-pd/al2o3 catalysts. *Energy Fuels* **2000**, *14*, 1205–1211.
9. Keith, L.H.; Telliard, W.A. Priority pollutants. I. A perspective view. *Environ. Sci. Technol.* **1979**, *13*, 416–423.
10. Agency for Toxic Substances and Disease Registry (ATSDR). *Toxicology Profile for Polyaromatic Hydrocarbons (CD-ROM)*; CRC Press: Boca Raton, FL, USA, 2005.

11. Sun, Z.; Zhang, H.; An, G.; Yang, G.; Liu, Z. Supercritical CO_2-facilitating large-scale synthesis of ceo_2 nanowires and their application for solvent-free selective hydrogenation of nitroarenes. *J. Mater. Chem.* **2010**, *20*, 1947–1952.

12. List, G.R.; King, J.W. *Hydrogenation of Fats and Oils: Theory and Practice*; AOCS Press: Urbana, IL, USA, 2011.

13. Kröcher, O.; Köppel, R.A.; Baiker, A. Sol-gel derived hybrid materials as heterogeneous catalysts for the synthesis of *n,n*-dimethylformamide from supercritical carbon dioxide. *Chem. Commun.* **1996**, 1497–1498.

14. Sahle-Demessie, E.; Gonzalez, M.A.; Enriquez, J.; Zhao, Q. Selective oxidation in supercritical carbon dioxide using clean oxidants. *Ind. Eng. Chem. Res.* **2000**, *39*, 4858–4864.

15. Stevens, J.G.; Bourne, R.A.; Twigg, M.V.; Poliakoff, M. Real-time product switching using a twin catalyst system for the hydrogenation of furfural in supercritical CO_2. *Angew. Chem. Int. Ed.* **2010**, *49*, 8856–8859.

16. Hitzler, M.G.; Smail, F.R.; Ross, S.K.; Poliakoff, M. Selective catalytic hydrogenation of organic compounds in supercritical fluids as a continuous process. *Org. Process Res. Dev.* **1998**, *2*, 137–146.

17. Arunajatesan, V.; Subramaniam, B.; Hutchenson, K.W.; Herkes, F.E. Fixed-bed hydrogenation of organic compounds in supercritical carbon dioxide. *Chem. Eng. Sci.* **2001**, *56*, 1363–1369.

18. Shirai, M.; Rode, C.V.; Mine, E.; Sasaki, A.; Sato, O.; Hiyoshi, N. Ring hydrogenation of naphthalene and 1-naphthol over supported metal catalysts in supercritical carbon dioxide solvent. *Catal. Today* **2006**, *115*, 248–253.

19. Hiyoshi, N.; Inoue, T.; Rode, C.V.; Sato, O.; Shirai, M. Tuning cis-decalin selectivity in naphthalene hydrogenation over carbon-supported rhodium catalyst under supercritical carbon dioxide. *Catal. Lett.* **2006**, *106*, 133–138.

20. Yuan, T.; Marshall, W.D. Catalytic hydrogenation of polycyclic aromatic hydrocarbons over palladium/γ-Al_2O_3 under mild conditions. *J. Hazard. Mater.* **2005**, *126*, 149–157.

21. Nelkenbaum, E.; Dror, I.; Berkowitz, B. Reductive hydrogenation of polycyclic aromatic hydrocarbons catalyzed by metalloporphyrins. *Chemosphere* **2007**, *68*, 210–217.

22. Houndonougbo, Y.; Jin, H.; Rajagopalan, B.; Wong, K.; Kuczera, K.; Subramaniam, B.; Laird, B. Phase equilibria in carbon dioxide expanded solvents: Experiments and molecular simulations. *J. Phys. Chem. B* **2006**, *110*, 13195–13202.

23. Cheng, Z.X.; Zhao, X.G.; Li, J.L.; Zhu, Q.M. Role of support in CO_2 reforming of CH4 over a Ni/γ-Al_2O_3 catalyst. *Appl. Catal. A* **2001**, *205*, 31–36.

24. Li, C.; Chen, Y.-W. Temperature-programmed reduction studies of nickel oxide/alumina catalysts: Effects of the preparation method. *Thermochim. Acta* **1995**, *256*, doi:10.1002/ls.3010130406.

25. Rynkowski, J.M.; Paryjczak, T.; Lenik, M. On the nature of oxidic phases in NiO/γ-Al_2O_3 catalysts. *Appl. Catal. A* **1993**, *106*, 73–82.

26. Wang, S.; Lu, G.Q. Reforming of methane with carbon dioxide over Ni/Al2O3 catalysts: Effect of nickel precursor. *Appl. Catal. A* **1998**, *169*, 271–280.

27. Mattos, M.; Souza, V.M.; Schmal, M. Supported Nickel catalysts for steam reforming of Methane. In *Proceedings of the 2nd Mercosur Congress on Chemical Engineering, 4th Mercosur Congress on Process Systems Engineering*, Rio de Janeiro, Brazil, 14–18 August 2005; ISBN 85-7650-043-4.

28. Pendrosa, A.M.G.; Souxa, M.J.B.; Melo, D.M.A.; Araujo, A.S. Cobalt and nickel supported on HY zeolite: Synthesis, characterization and catalytic properties. *Res. Bull.* **2006**, *41*, 1105–1111.

29. Hampson, J.W. A recirculating equilibrium procedure for determining organic compound solubility in supercritical fluids. Anthracene in carbon dioxide. *J. Chem. Eng. Data* **1996**, *41*, 97–100.

30. Ashraf-Khorassani, M.; Combs, M.T.; Taylor, L.T.; Schweighardt, F.K.; Mathias, P.S. Solubility study of sulfamethazine and sulfadimethoxine in supercritical carbon dioxide, fluoroform, and subcritical freon 134A. *J. Chem. Eng. Data* **1997**, *42*, 636–640.

31. Hiyoshi, N.; Rode, C.V.; Sato, O.; Shirai, M. Biphenyl hydrogenation over supported transition metal catalysts under supercritical carbon dioxide solvent. *Appl. Catal. A* **2005**, *288*, 43–47.

32. Aizawa, T.; Janttarakeeree, S.; Ikushima, Y.; Saitoh, N.; Arai, K.; Smith, R., Jr. Cosolvent effect on enhancement of reaction rate constant in near-critical region. *J. Supercrit. Fluids* **2003**, *27*, 247–253.